Enhancing the capability of future medium-size telescopes: First light of the SALTO demonstrator

Jyotirmay PAUL[1,*], Gilles ORBAN DE XIVRY[1], Olivier ABSIL[1], Cédric ADAM[2], Pierre ALBART[2], Christian BASTIN[2], Alice BOULANGER[2], Jonathan DE VILLE[2], Eric GABRIEL[2], Laurence MÉANT[2], Vincent MOREAU[2], Sabrina ORBAN[2], Pierre REMACLE[2], Fabian LANGUY[3], Marc GEORGES[3], Jean-François VANDENRIJT[3], Gabriel MILLOU[3], Claude NIGOT[4] and Vincenzo CARAMIA[4]

[1] Space sciences, Technologies, and Astrophysics Research (STAR) Institute, Université de Liège, Belgium
[2] Advanced Mechanical and Optical System (AMOS), Liège, Belgium
[3] Centre Spatial de Liège (CSL), Université de Liège, Belgium
[4] Redu Space Services (RSS), Redu, Belgium
[*] Corresponding author: jpaul@uliege.be

Abstract

The adaptive optics (AO) technology is crucial to achieve the full potential of ground-based telescopes. Over the last three decades, the world has witnessed the successful advent and operation of AO systems on large ground-based telescopes. The complexity and cost of AO systems have largely gone down in the last decade thanks to advances in deformable mirror, wavefront sensor, and real-time computing technologies. Here, we present a robust Rayleigh scattered laser-guided single conjugated adaptive optics system called SALTO, which was designed, built, and tested in the Belgian countryside on a 1-meter class telescope. This project aims to demonstrate the possibility of rejuvenating the scientific goals of medium-class telescopes (1-3 m) with AO technology, as well as to enable optical telecommunication from relatively poor observing sites. This paper discusses the overview of the design, integration and calibration of SALTO. It concludes with the presentation of successful on-sky results at 1.55μm under 2-3$''$ seeing.

Keywords: atmospheric effects, adaptive optics, laser guide star, high angular resolution

1. Introduction

Adaptive optics (AO), (Babcock, 1953) is an influential technology employed to mitigate the adverse impacts of atmospheric turbulence on astronomical observations. Turbulence within the Earth's atmosphere induces rapid fluctuations in the refractive index caused by solar heating,

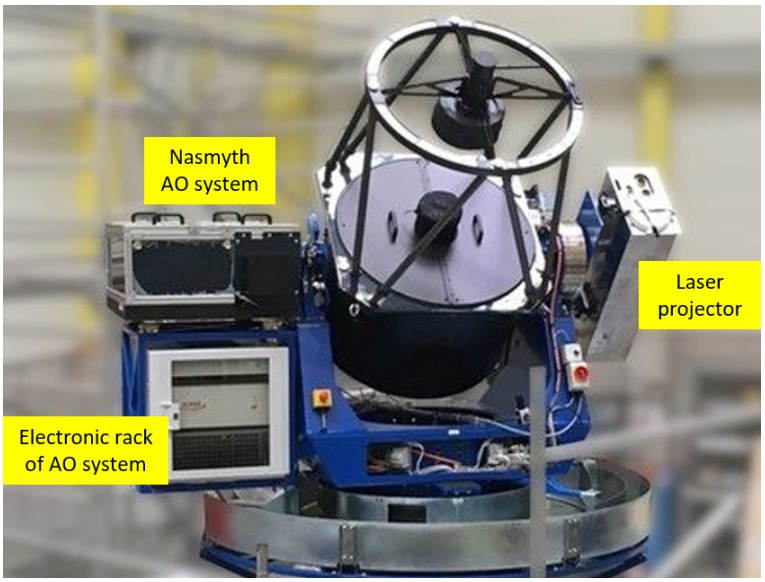

Figure 1: Entire SALTO with Laser projector at AMOS integration hall (PC: AMOS).

resulting in a time-varying phase disturbance in the incident light wavefront from celestial objects. This phase distortion hampers spatial resolution and sensitivity, imposing limitations on the capabilities of ground-based telescopes (Hardy, 1998). AO systems employ one or multiple deformable mirrors to swiftly introduce a compensatory phase, thereby correcting the wavefront and producing diffraction-limited images. Over the past few decades, AO has become an indispensable part of numerous astronomical telescopes, enabling deeper exploration of the celestial sphere. Despite the availability of AO technology, its implementation in medium-class telescopes has been limited due to cost constraints. Nevertheless, there are numerous medium-class telescopes worldwide capable of supporting and conducting follow-up observations for large sky surveys such as GAIA (Gaia Collaboration, 2016), PLATO (Rauer and Catala, 2014) etc. To enhance the sensitivity and capabilities of these telescopes, affordable and low-overhead AO systems like Robo-AO (Baranec et al., 2013), iRobo-AO (Paul et al., 2019) etc. have been developed. The Smart Adaptive-optics and Laser guide-star for medium-size Telescopes and Optical communications (SALTO) project serves as a pilot initiative aimed at revitalizing medium-class telescopes and demonstrating space-to-ground optical communication using 1-meter class telescopes with laser beacons (Fig. 1).

The primary objective of this paper is to present the design leading up to the first light of SALTO. While a substantial portion of this work has already been published in a recent publication by Orban de Xivry et al. (2022), the present paper primarily focuses on presenting and explaining specific aspects, including the optical relay, the calibration unit, the range gate unit, and the latest results achieved using both natural guide star (NGS) and laser guide star (LGS) techniques. In the second section, we provide an overview of the entire system. Section three is dedicated to discussing the software architecture and AO control method. Section four focuses on system calibration. Lastly, in section five, we conclude with the commissioning and the first light of SALTO.

2. Overview of the entire SALTO system

The SALTO system is a single-conjugate adaptive optics (SCAO) system that encompasses several subsystems, including the telescope, Nasmyth AO table, calibration unit, range gate system, laser projector, software architecture, real-time controller, and more. In this paper, we provide detailed descriptions of each of these subsystems.

2.1. Telescope

The AO system is installed on the Nasmyth platform of an 800 mm Ritchey-Chrétien telescope, which has been designed and developed by AMOS. The laser projector is mounted on the opposite side of the Nasmyth platform, while the electronic rack is mounted beneath the AO system. The telescope's carbon fiber tube effectively reduces weight and minimizes the obstruction caused by the spider. The robust structure of the telescope is capable of supporting the AO system, electronics rack, and projector. The telescope has a focal ratio of 7.5, a linear obscuration of 35%, and a 20 $'$ field-of-view (FoV) diameter. The primary mirror possesses a surface figure error of 35 nm rms and is coated with protected aluminum, ensuring a minimum reflectivity of 95% at 532 nm. Due to its finite height of the LGS, the telescope produces an image of the LGS located 3.6 mm away from the focal plane.

2.2. Description of AO design and integration

The design of the Nasmyth AO facility holds great importance as it emphasizes the selection of off-the-shelf optics and optomechanical components. This approach ensures affordability for medium-class observatories and facilitates easy replication. The system is specifically tailored to handle significant atmospheric turbulence (2"-4") encountered in rural areas of Belgium. A comprehensive simulation utilizing AOtools (Townson et al., 2019) and soapy (https://github.com/AOtools/aotools and https://github.com/AOtools/soapy) was conducted, and all the specifics can be found in (Orban de Xivry et al., 2019, 2018). The Nasmyth AO facility is composed of two arms: a science arm that operates in the near-infrared (1-1.7 μm) regime and a wavefront sensing arm that operates in the visible regime ($\sim$ 532 nm). The science camera has a FoV of 1$'$ diameter, and the wavefront sensing (WFS) camera has a FoV of 12.5" diameter (FoV corresponds to one sub-aperture at the WFS camera). To overcome the FoV constraint at the science camera for pointing the telescope, a wide-field camera with a FoV of $\sim 20'$ is integrated into the system. A calibration unit (i.e. telescope simulator) is an integral part of the SALTO for system alignment, integration, calibration and testing and the details are presented later. The optical relay in the integrated Nasmyth table facility is depicted in Fig. 2. It includes three off-axis parabolic (OAP) mirrors, a deformable mirror (DM), a dichroic mirror, near infrared (NIR) camera, range gate unit, Shack-Hartmann wavefront sensor (SHWFS), a high-speed WFS camera, several fold mirrors etc. ALPAO 97 DM with 11 $\times$11 array of actuators is employed and it has the capacity to correct for tip-tilt and high-order aberrations of the atmosphere in moderate seeing conditions (2"-4").

Here, the optical ray tracing for Fig. 2 is provided. The telescope directs both the science

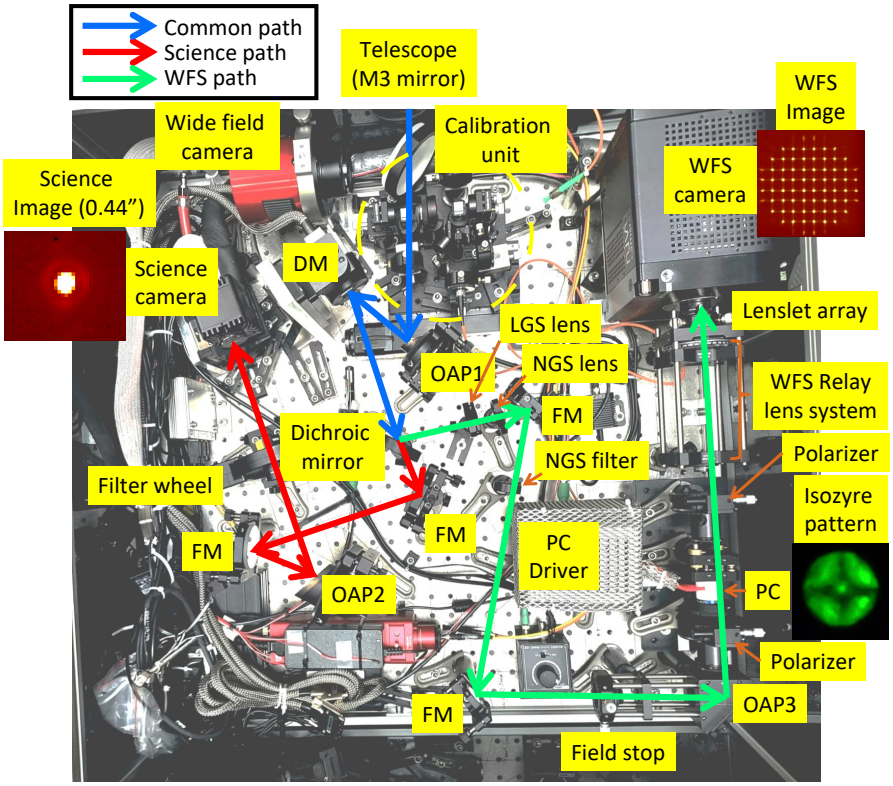

Figure 2: SALTO Nasmyth Table (Blue path: Telescope's entire light; Green path: WFS path; Red path: Science path).

and wavefront sensing beams along a common trajectory, initially striking off-axis parabolic mirror (OAP) tagged as OAP1, followed by the DM and dichroic mirror (only reflects 400-633 nm), as illustrated in blue. This segment of the entire optical train made up of OAP1, the DM, and the dichroic mirror, is shared by both the science and the wavefront sensing arms upto the bifurcation by the dichroic mirror. At the dichroic mirror, near-infrared light is transmitted to the science path (shown in red), while the visible light is reflected towards the WFS path (green). Subsequently, the science beam undergoes reflection via a pair of flat mirrors (FM), reflects on another OAP marked as OAP2, with an equivalent off-axis distance to OAP1 to create an intermediate image of the target with minimal aberration. The beam proceeds through a pair of relay lenses to generate a science image such that the intermediate image is magnified to meet the Nyquist sampling criteria at the C-RED science camera. The facility features the InGaS C-RED3 NIR camera (First Light, 640×512, 15μm pixel size, wavelength range 900-1700 nm) for science observations. An automated filter wheel with several filters is also used for photometry in different bands. The both lenses of the relay are mounted on either side of the filter wheel aperture to eliminate the space constraint. On the WFS path, the collimated WFS beam is subsequently focused at the back focal plane of OAP3 by either the LGS or NGS lens, depending on the operational mode and steered by a sequence of two flat mirrors. The both LGS and NGS lenses are mounted but only one is utilized to generate an intermediate image of the guide star. One lens is dedicated to the NGS mode, while the other is employed for the LGS mode. To facilitate effortless mode switching, these lenses are securely affixed to a

quick-release magnetic mount. In the LGS mode, an ultra-narrow filter at 532 nm is integrated into the LGS lens mount, effectively eliminating unwanted light and permitting only the laser-backscattered light to transmit. Contrarily, in the NGS mode, a broadband filter with a central wavelength of 560 nm and a half-bandwidth of 120 nm is placed between the two FMs. This broader bandwidth enhances the acquisition of NGS WFS photons, resulting in an increased Signal-to-Noise Ratio (SNR) and an enhancement in the precision of wavefront measurements. Additionally, a field stop is positioned at the intermediate focal plane. The purpose of the field stop serves two-fold: to restrict the size of the guide star to prevent spillover into the adjacent subaperture and to obstruct the stray light entering the WFS camera caused by backscattering from the lower altitudes of the laser beacon. Beyond this point, the WFS beam diverges, and then the OAP3 collimates the intermediate-focused beam and generates a pupil again. It then passes through a range gate. The range gate is mounted at this pupil and further discussion about it is given at the end of this section. The beam proceeds through another pair of lenses and eventually reaches on the lenslet array. The pair of lenses is used as a relay lens system to demagnify the beam to match the pupil size projected onto the 10×10 lenslet array. The eventually the WFS beam reaches on the lenslet array and finally, the array of focused images of the guide star is captured by the WFS camera. The heart of the wavefront sensing arm is a fast-readout, wavefront sensing Nüvü camera (green-light-sensitive EMCCD, 128×128, 1 kHz, $<1e^-$ RON) and a Shack-Hartmann lenslet array of 10×10. The lenslet array, SHWFS, and DM are aligned according to Fried geometry for efficient wavefront sensing. The complete system is constructed on an optical table with a honeycomb structure and shielded by a protective box measuring approximately $\sim$ 750 mm $\times$ 750 mm $\times$ 300 mm in size.

2.3. Calibration unit

Calibration unit generates an identical telescope beam. The SALTO system is designed to operate initially with the NGS and then move on to the LGS mode, enabling permanent all-sky coverage. In order to accommodate both guide stars, the calibration unit incorporates three arms. Two of these arms are specifically designed to generate NGS and LGS guide stars for wavefront sensing purposes, while the third arm is dedicated to NGS science observations. A unit magnification setup is employed, employing identical focal lengths of collimator and camera. The light is relayed using a pair of beamsplitters. Fiber fed sources are used. The NGS science source fiber remains fixed at the back focal plane of one collimator (concave mirror) as primary source. The NGS and LGS are used as guiding sources for wavefront sensing, sharing a collimating lens. Both NGS and LGS wavefront sensing fiber tips are at the focal plane and 3.6 mm inside of the focal plane of the collimating lens respectively to simulate the telescope's both focal planes.

The optical ray tracing of the calibration unit is also given here. Within the schematic diagram (Fig. 3), it can be observed the trajectories of three distinct beams: the NGS WFS, LGS WFS, and NGS science beams, represented by blue, green, and red lines, respectively. The light originating from both the NGS WFS and LGS WFS sources follows almost the same path, ultimately reaching the concave camera mirror. This journey involves a sequence of reflection

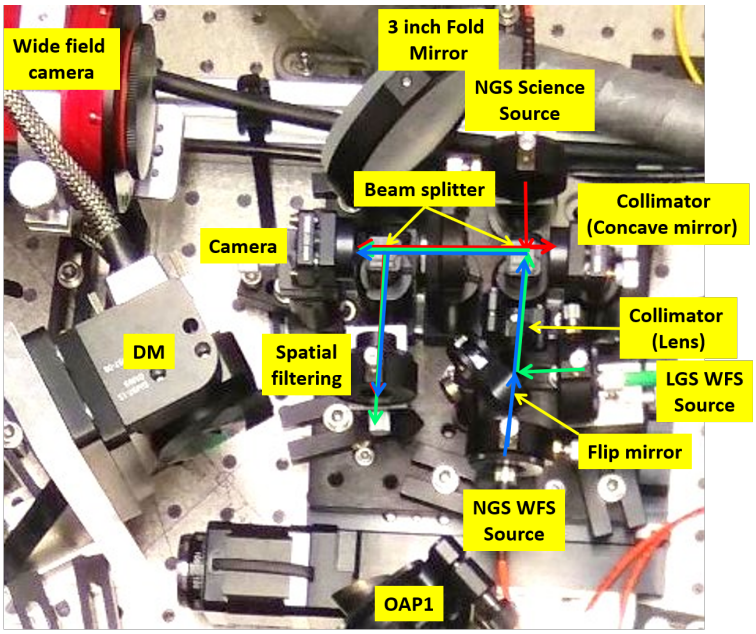

Figure 3: SALTO Calibration unit.

from the first beam splitter and subsequent transmission through the second beam splitter. A 90-degree flip mirror is positioned between the WFS sources and the collimating lens, allowing us to switch between NGS and LGS WFS modes seamlessly. On the other hand, the NGS science beam takes a slightly different path until it is collimated. After reflecting of the first beam splitter, it is directed towards the collimating concave mirror. It then proceeds through both beam splitters along the WFS beams before striking the concave camera mirror. This intricate optical relay yields the generation of NGS science and WFS images at the telescope focal plane, along with the LGS WFS image positioned 3.6 mm away from the focal plane. The entire calibration unit is mounted on a computer-controlled linear translating stage, which can be adjusted for calibration or removed to allow sky light into the system.

2.4. Range gate unit

The range gate system is designed with the philosophy of constructing an optical high-speed shutter to facilitate the capture of Rayleigh backscattered photons from a specific air slab located at a predetermined altitude of $\sim$10 km, where the laser projector focuses the laser. The optical shutter consists of a pockel cell (PC) made of a KTP crystal sandwiched between two crossed Glan-Taylor polarizers, operating at a wavelength of 532 nm (Fig. 2). The KTP crystal exhibits a half-wave plate (HWP) property under approximately $\sim$1 kV, and the entire system enables a high rejection ratio against stray backscattered light. The synchronization between the laser pulse and the optical shutter is achieved using a pulse generator referred to as the Master Clock. This master clock sends an initial trigger pulse to launch a laser pulse, followed by a subsequent delayed trigger pulse to activate the KTP crystal, inducing its HWP property. The applied delay corresponds to the round-trip travel time of the light required to reach the designed altitude. This, in turn, opens the optical shutter of the range gate system. Additionally, another

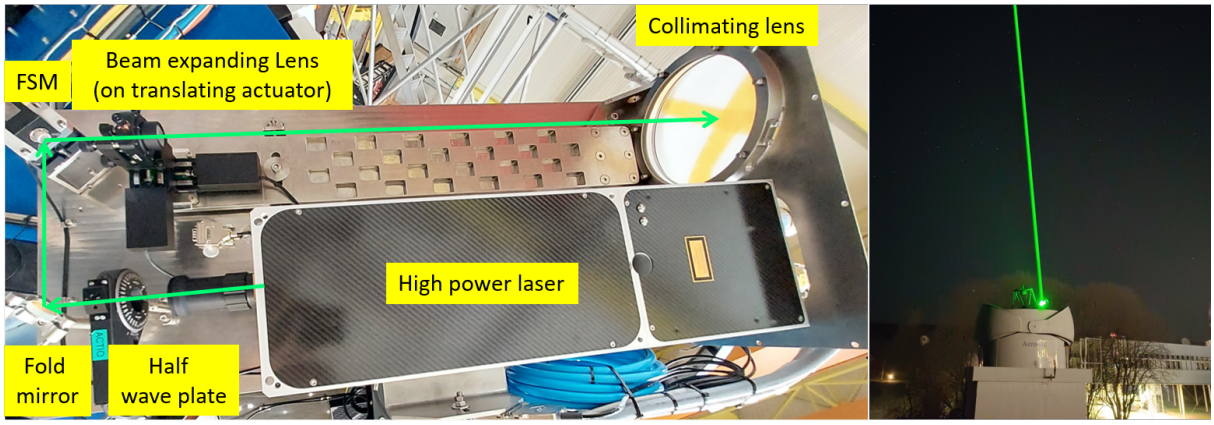

Figure 4: (left) Depiction of the integrated Laser Launch System following its integration with the telescope. (right) Laser propagation in the sky in high power at Redu.

delayed trigger pulse is sent to close the optical shutter. The system achieves fast opening times ranging from under 2 μs to 10 μs, corresponding to air slab thicknesses between 300 m and 1500 m. The KTP crystal is meticulously aligned using the help of the symmetricity of the isogyre pattern, with its central spot. It is produced by inserting a diffuser in front of the PC.

2.5. Laser projector

Laser guide stars (LGSs) have revolutionized AO by allowing ground-based telescopes to achieve near-diffraction-limited performance all over the sky. The creation of an artificial star in the Earth's upper atmosphere using a laser beam is the key to LGSs. The SALTO projects the laser beam in the sky by the laser projector unit, and generates a LGS through the utilization of Rayleigh scattering. The core part of this unit is a high power (18 watt), 532 nm pulsed laser (a pulsation rate of 10 kHz, and a pulse width of 40 ns, beam quality factor >1.3 TEM_{00}). The laser projector expands and refocuses the laser at 10 km altitude using an afocal system to prevent plasma creation inside it (Clermont et al., 2020). Fig. 4 presents a comprehensive illustration of the laser projector and the propagation of laser beams in the sky.

The optical path is illustrated in green. The high-power laser source emits a high-power pencil beam. This pencil beam passes through a half-wave plate, to control the polarization orientation to maximize backscattered photon throughput in the range gate system. The beam is subsequently redirected by a pair of flat mirrors, with the second mirror being referred to as the fast steering mirror (FSM) to control the direction of the laser projection. Moreover, the pencil beam also passes through an external safety shutter, in addition to the internal laser shutter, as an additional safety precaution. At the end, the laser beam is expanded by a beam-expanding lens before the collimating lens launches the beam into the sky.

3. Software architecture and AO control method

The real-time computer (RTC) of SALTO is a in-house software (in C/C++ and Python) with cacao package data stream approach (Guyon et al., 2018, 2020) which incorporates meta-data, pointers to shared memory holding the data, semaphore pointers etc. The operational process is as follows: when a process writes data to a data stream, the associated semaphores are incremented. This prompts any downstream process waiting for these semaphores to proceed immediately, subsequently reducing the semaphore value. Our control loop is constructed based on this data format and inter-process communication (IPC) mechanism. To ensure ease of implementation, all real-time and soft real-time processes are developed using Python, and the hardware interfaces are implemented in C/C++. Several shared memory contains various data, including the WFS image, wavefront slope vector, and DM commands. The AO pipeline continuously calculates the wavefront slope by analyzing new WFS images retrieved from the shared memory. The slope of the wavefront at each subaperture is estimated using the center of gravity algorithm of the WFS spots. The pipeline takes care of flux normalization across the entire aperture to reduce noise propagation and intensity threshold. Once the slope offset has been subtracted from the initially estimated slopes, the slope vector within the shared memory object is then updated. The slope vectors undergo multiplication with the reconstruction matrix, followed by the mode to command matrix, and pass through a leaky integrator (Madec and Roddier, 1999). This process generates the DM commands, which are stored in one of the four DM shared memory channels. As per safety norms the high commands undergo clipping to the maximum allowable value. Once the DM commands are available in the channels, they are combined, and the DM is triggered as soon as a new value is received in any of the channels. This multi-channel approach address various aspects, i.e. DM's flat map, tip-tilt commands, and real-time disturbance for daytime calibration. TCS offloading is performed to avoid the accumulation of a large amount of tip-tilt at the DM. In LGS mode the tip-tilt values are computed from the science camera. On the other hand, the tip-tilt calculated from the LGS WFS is due to laser pointing inaccuracy, vibration, the double pass of the beam through the atmosphere etc. which is eliminated and then fed to one of the DM channel. The eliminated tip-tilt from WFS is then applied to the FSM of the laser projector.

4. System calibration

The calibration process of the AO system and the control of the deformable mirror (DM) are done using the calibration unit. To generate the modal basis for controlling the 97 actuators of the DM, a combination of theoretical Karhunen-Loève (KL) modes, measured influence functions, and pupil definition are employed. The construction of the basis involves three steps: construction of the theoretical KL modes, projecting the theoretical basis onto the influence functions, and calculating the fitted modal basis. Following this approach we obtained 66 KL modal basis for the 97 actuators of the ALPAO DM and used for for onsky. The interaction matrix, denoted as M, between the DM and the wavefront sensor (WFS), is acquired using the push-pull technique in the modal space. The computation of the jth column of M involves determining the WFS slope vector (S) associated with the jth mode (m_j).

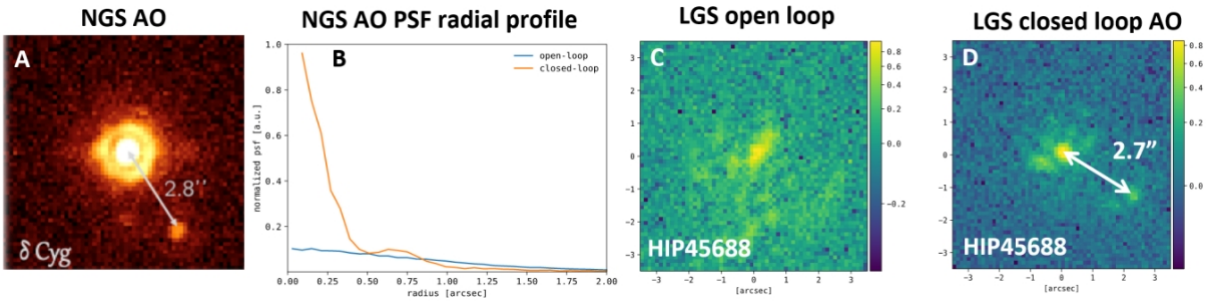

Figure 5: (A) An image of the delta Cygnus star taken with a 15-second exposure. The image shows delta Cygnus B, which is located approximately 2.8" away from the main star. (Image taken from Orban de Xivry et al. (2022)) (B) A comparison of the radial profiles between closed-loop (shown in orange) and open-loop (shown in blue) observations. These profiles were obtained during the initial night using point spread functions (PSFs) generated from 15 seconds of integration time at a wavelength of 1.55μm. The peak intensity is 6 times higher in closed loop. (Image taken from Orban de Xivry et al. (2022)) (C-D) Short-exposure images of a binary star, with the companion star located 2.7" away (HIP45688). These images were captured with a 0.2-second exposure with an open-loop PSF at 10-second intervals (C) and a closed-loop PSF (D), respectively.

$$M(j) = \frac{S(+Am_j) - S(-Am_j)}{2A} \tag{1}$$

where A is an amplitude vector, which we tune to have a uniform response across all modes. A sanity check is performed by examining the noise covariance matrix, $(M^T M)^{-1}$, and then the reconstructor is computed via pseudo-inversion of the M.

5. Commissioning and first light

After its development at the STAR institute, the entire AO system was relocated to the telescope floor for system integration and commissioning. Following the completion of system integration, we replaced the existing lenslet array with a high-transmission alternative. We then performed precise realignment of the lenslet array to ensure Fried geometry between the DM and the lenslet array at the telescope. The alignment was fine-tuned to maximize the symmetry of the WFS response. It was discovered that the mapping between the telescope pupil and the deformable mirror plane is slightly misaligned by approximately 5-10% of the pupil diameter after integrating the AO table with the telescope. It was rectified subsequently. During initial operation (at the end of 2021), we successfully closed the AO loop on a NGS, controlling 30 KL modes at 100 Hz framerate. From a seeing condition of 2", we were able to achieve the diffraction limit of 0.4" at a wavelength of 1.55 μm. Fig. 5A and 5B shows the resulting PSF obtained during observations of delta Cygnus with a 15-second integration time. The

radial profile (Fig. 5B) demonstrated more than a six-fold increase in peak intensity. During the following nights, our primary emphasis was on refining AO operations, addressing control-related aspects etc. We accomplished enhanced system robustness, improved performance, and achieved a better Strehl ratio by effectively correcting up to 66 KL modes and operating at a high frame rate of 500 Hz in NGS mode.

By the end of 2022, we obtained the necessary authorization to propagate the laser at its maximum power (18 W) (refer to Fig. 4). Following a series of technical interventions, we conducted a comprehensive laser test on sky in December at Redu Space Services. Remarkably, we were able to achieve closed-loop AO operation on a laser guide star, at a relatively low frame rate of 20 Hz. In this setup, the LGS tip-tilt was directly corrected by the deformable mirror (DM) itself, rather than relying on the FSM of the laser projector. Additionally, the atmospheric tip-tilt was compensated during post-processing by employing a simple shift-and-add technique. Ultimately, we achieved a modest but notable level of correction, as evidenced by the distinct and well-defined central diffraction-limited core visible in the LGS closed-loop PSF (Fig. 5D) wrt. open loop PSF (Fig. 5C).

Acknowledgments

The authors would like to express their gratitude for the support received from the Walloon region of Belgium through the Skywin program (project SALTO). Additionally, OA acknowledges the support from the Belgian national funds for scientific research (FNRS).

Further Information

ORCID identifiers of the authors

0009-0001-2752-5072 (Jyotirmay PAUL)
0000-0002-4790-415X (Gilles ORBAN DE XIVRY)
0000-0002-4006-6237 (Olivier ABSIL)

Author contributions

J. Paul was involved in the entire process of optical alignment, integration, testing of the Nasmyth AO table and the calibration unit, system calibration, cabling, plumbing, procurement, commissioning, and other related tasks. G. Orban de Xivry lead the development of the AO system, and performed seeing measurements, simulations, optical design, procurement, software development, calibration, commissioning, among others. O. Absil provided support and advises for the conceptualization and realization of the AO system. J-F Vandenrijt and F. Languy were responsible for developing the laser projector system and associated software for the laser controller. G. Millou handled the optical alignment and testing of the range gate system. The AMOS team was project lead and responsible for the telescope, commissioning, and

electronic racks. V. Caramia and C. Nigot from Redu Space Services provided on-site infrastructure and comprehensive support at Redu. All authors made contributions in the meetings and preparation of this manuscript.

Conflicts of interest

The authors declare no conflict of interest.

References

Babcock, H. W. (1953) The possibility of compensating astronomical seeing. PASP, 65(386), 229. https://doi.org/10.1086/126606.

Baranec, C., Riddle, R., Law, N. M., Ramaprakash, A. N., Tendulkar, S. P., Bui, K., Burse, M. P., Chordia, P., Das, H. K., Davis, J. T. C., Dekany, R. G., Kasliwal, M. M., Kulkarni, S. R., Morton, T. D., Ofek, E. O. and Punnadi, S. (2013) Bringing the Visible Universe into Focus with Robo-AO. JVE, 72. https://doi.org/10.3791/50021.

Clermont, L., Languy, F. and Georges, M. P. (2020) Afocal combinations and focus control for laser launch telescopes. JATIS, 6(3), 034003. https://doi.org/10.1117/1.JATIS.6.3.034003.

Gaia Collaboration (2016) The Gaia mission. A&A, 595, A1. https://doi.org/10.1051/0004-6361/201629272.

Guyon, O., Sevin, A., Ferreira, F., Ltaief, H., Males, J., Deo, V., Gratadour, D., Cetre, S., Martinache, F., Lozi, J., Vievard, S., Fruitwala, N., Bos, S. and Skaf, N. (2020) Adaptive optics real-time control with the compute and control for adaptive optics (Cacao) software framework. SPIE, 11448, 2N. https://doi.org/10.1117/12.2562822.

Guyon, O., Sevin, A., Gratadour, D., Bernard, J., Ltaief, H., Sukkari, D., Cetre, S., Skaf, N., Lozi, J., Martinache, F., Clergeon, C., Norris, B., Wong, A. and Males, J. (2018) The compute and control for adaptive optics (CACAO) real-time control software package. SPIE, 10703, 1E. https://doi.org/10.1117/12.2314315.

Hardy, J. W. (1998) Adaptive Optics for Astronomical Telescopes. Oxford University Press.

Madec, P. Y. and Roddier, F. (1999) Control techniques. In Adaptive optics in astronomy, p. 131. Cambridge University Press. https://ui.adsabs.harvard.edu/abs/1999aoa..book.....R.

Orban de Xivry, G., Absil, O., Lismont, M., Moreau, V., Languy, F. and Vanhoenacker-Janvier, D. (2018) Preliminary design of SALTO: the Belgian adaptive optics demonstrator. SPIE, 10703, 38. https://doi.org/10.1117/12.2313578.

Orban de Xivry, G., Absil, O. and Moreau, V. (2019) A sharp future for the 3.6-m DOT? The power of adaptive optics for medium size telescopes. BSRSL, 88, 55–64.

Orban de Xivry, G., Paul, J., Absil, O., Adam, C., Albart, P., Bastin, C., Boulanger, A., de Ville, J., Gabriel, E., Méant, L., Moreau, V., Orban, S., Remacle, P., Languy, F., Georges, M., Vandenrijt, J. F., Millou, G., Nigot, C. and Caramia, V. (2022) Status of the SALTO demonstrator: project overview and first on-sky operations. SPIE, 12185, 34. https://doi.org/10.1117/12.2627936.

Paul, J., Das, H. K., Ramaprakash, A. N., Burse, M. P., Chordia, P. A., Chillal, K., Datir, G., Joshi, B., Khodade, P., Kohok, A., Mestry, V., Punnadi, S. P., Rajarshi, C. V. and Shekhar, C. (2019) Design and development of an adaptive optics system in visible and near-infrared for Inter-University Centre for Astronomy and Astrophysics 2-meter telescope. JATIS, 5(3), 039002. https://doi.org/10.1117/1.JATIS.5.3.039002.

Rauer, H. and Catala (2014) The PLATO 2.0 mission. ExA, 38(1-2), 249–330. https://doi.org/10.1007/s10686-014-9383-4.

Townson, M. J., Farley, O. J. D., de Xivry, G. O., Osborn, J. and Reeves, A. P. (2019) Aotools - a python package for adaptive optics modelling and analysis. OExpr, 27(22), 31316–31329. http://dro.dur.ac.uk/29348/.